Microgonotropens and Their Interactions with DNA. 5.[1] Structural Characterization of the 1:1 Complex of $d(CGCAAATTTGCG)_2$ and Tren-Microgonotropen-b by 2D NMR Spectroscopy and Restrained Molecular Modeling

Andrei Blaskó, Kenneth A. Browne, and Thomas C. Bruice*

Contribution from the Department of Chemistry, University of California, Santa Barbara, California 93106

Received October 27, 1993®

Abstract: Tren-microgonotropen-b (**6b**) binds 1:1 and 2:1 into the minor groove of $d(CGCAAATTTGCG)_2$. The solution structure of the 1:1 complex of $d(CGCA_3T_3GCG)_2$ with **6b** has been determined by 2D nuclear Overhauser effect ^1H NMR spectroscopy (NOESY) and restrained molecular modeling. An ^1H NMR melting study on $d(CGCA_3T_3GCG)_2$ shows that while the G·C base pairs exist equally as paired and melted forms of 35 °C, the A_3T_3 region maintains base pairing up to 45 °C. A total of 206 resonances for the $d(CGCA_3T_3GCG)_2$:**6b** have been assigned. The signals of both exchangeable and nonexchangeable protons in the NOESY spectra indicate asymmetric binding of **6b** in the A + T-rich region involving five base pairs ($5'$-$A_6T_7T_8T_9G_{10}$-$3'$). The terminal acetamide head of **6b** is directed toward A_6, while the carboxy terminal dimethylpropylamino tail is directed toward G_{10}. The protonated tren polyamino substituent residing on the nitrogen of the central pyrrole ring is directed up toward the phosphate backbone, firmly grasping the phosphodiester linkages of P_9 and P_{10} on the edge of the major groove. The protonated terminal nitrogen of the dimethylpropylamino tail is adjacent to sugar oxygen $C_{11}O4'$ and a base oxygen $C_{11}O2$ within the minor groove. The off-rate of **6b** from the 1:1 complex was found to be 1.3 ± 0.2 s^{-1}, corresponding to an activation energy of 17 kcal/mol. Compound **6b** binds 3.1–4.5 Å from the bottom of the minor groove and 7.3–9.0 and 5.5–6.4 Å distant from the (–) and (+) strands, respectively when observing the strands of the DNA in a 5′ to 3′ orientation (distances from the pyrrole nitrogens to $P_{-4}P_{-5}P_{-6}$ and $P_8P_9P_{10}$, respectively). Comparisons of the solution structures of $d(CGCA_3T_3GCG)_2$ and the $d(CGCA_3T_3GCG)_2$:**6b** complex with the crystal structure of the same dsDNA, show that there is a break in the C_{2v} symmetry of the crystallized dsDNA at the A_6T_7 junction as it goes into aqueous solution. A helical bend, α, of 22.2° was found for the solution structure of the $d(CGCA_3T_3GCG)_2$:**6b** complex; this is an increase of 11.4° relative to the crystallized dodecamer (α = 10.8°), 8.3° relative to the crystallized $d(CGCA_3T_3GCG)_2$:distamycin complex (α = 13.9°) and 5.0° relative to the solution structure of $d(CGCA_3T_3GCG)_2$:**5c** complex (α = 17.2°). In addition, solvation increases the length of the duplex by 0.2 Å/bp for the $d(CGCA_3T_3GCG)_2$:**6b** complex compared to crystal structures of $d(CGCA_3T_3GCG)_2$ and of the $d(CGCA_3T_3GCG)_2$:distamycin complex. The A·T region of the $d(CGCA_3T_3GCG)_2$:**6b** complex maintains its B-DNA conformation, while the terminal G·C ends appear to exist in an intermediate B- to A-DNA form.

Introduction

Agents which bind to the minor groove of dsDNA and extend to the major grove have been designed and synthetized[2a] under the name of microgonotropens.[2c] Dien-microgonotropen (**5**) and tren-microgonotropen (**6**) structures are compared in Chart 1. Microgonotropens, like the related lexitropsin minor groove binding agents distamycin and netropsin, have an affinity for A + T-rich regions.[2a–e,3] The dodecamer $d(CGCAAATTTGCG)_2$ with its A_3T_3 center unit can accommodate one molecule of berenil or pentamidine,[4a] two molecules of Hoechst 33258,[3] and two[5] or four[6] molecules of distamycin in antiparallel modes of binding. Heterocomplexation of distamycin and 2-imidazole-distamycin[4b] by $d(CGCAAGTTGGC)/d(GCCAACTTGCG)$ has been reported. The main feature common to these molecules is a "sickle-

Chart 1

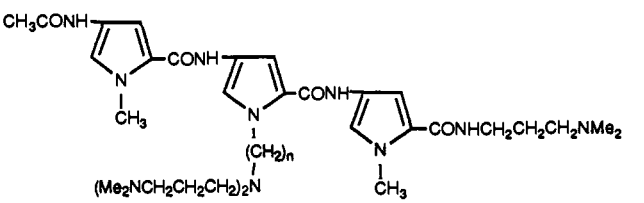

5a, n=3; **5b**, n=4; **5c**, n=5

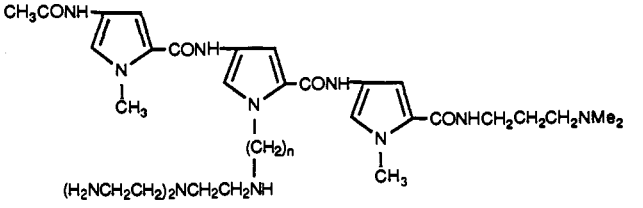

6a, n=3; **6b**, n=4; **6c**, n=5

* Abstract published in *Advance ACS Abstracts*, March 15, 1994.

(1) Chemistry of Phosphodiesters, DNA and Models. 7. Part 1: ref 2a. Part 2: ref 2b. Part 3: ref 2c. Part 4: ref 2d. Part 5: ref 2e. Part 6: ref 3.

(2) (a) Bruice, T. C.; Mei, H.-Y.; He, G.-X.; Lopez, V. *Proc. Natl. Acad. Sci. U.S.A.* **1992**, *89*, 1700. (b) Browne, K. A.; Bruice, T. C. *J. Am. Chem. Soc.* **1992**, *114*, 4951. (c) He, G.-X.; Browne, K. A.; Groppe, J. C.; Blaskó, A.; Mei, H.-Y.; Bruice, T. C. *J. Am. Chem. Soc.* **1993**, *115*, 7061. (d) Browne, K. A.; He, G.-X.; Bruice, T. C. *J. Am. Chem. Soc.* **1993**, *115*, 7072. (e) Blaskó, A.; Browne, K. A.; He, G.-X.; Bruice, T. C. *J. Am. Chem. Soc.* **1993**, *115*, 7080.

(3) He, G.-X.; Browne, K. A.; Blaskó, A.; Bruice, T. C. *J. Am. Chem. Soc.* **1994**, first of two papers in this issue.

(4) (a) Jenkins, T. C.; Lane, A. N.; Neidle, S.; Brown, D. G. *Eur. J. Biochem.* **1993**, *213*, 1175. (b) Geierstanger, B. H.; Dwyer, T. J.; Bathini, Y.; Lown, J. W.; Wemmer, D. E. *J. Am. Chem. Soc.* **1993**, *115*, 4474.

(5) Pelton, J. G.; Wemmer, D. E. *J. Am. Chem. Soc.* **1990**, *112*, 1393.

(6) Blaskó, A.; Bruice, T. C. *Proc. Natl. Acad. Sci. U.S.A.* **1993**, *90*, 10018.

0002-7863/94/1516-3726$04.50/0

Chart 2

a

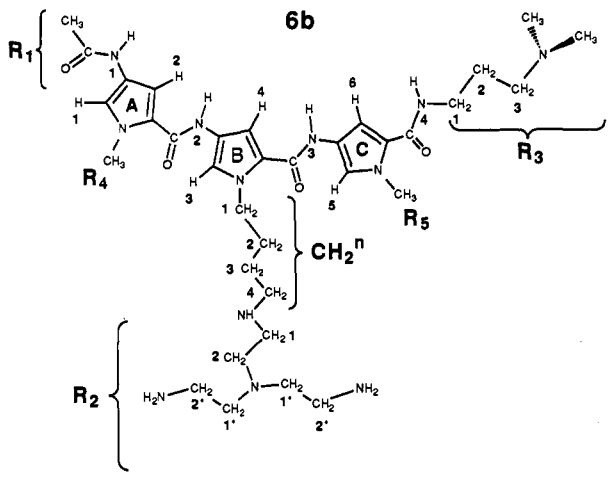

b

5'- C_1 G_2 C_3 A_4 A_5 A_6 T_7 T_8 T_9 G_{10} C_{11} G_{12} -3'

3'- G_{-1} C_{-2} G_{-3} T_{-4} T_{-5} T_{-6} A_{-7} A_{-8} A_{-9} C_{-10} G_{-11} C_{-12} -5'

shape" which facilitates binding in the minor groove of B-DNA. The central polyamine substituents of the microgonotropens were designed to reach the phosphate backbone of DNA, to point toward the major groove, and be able to ligate a metal ion, thereby providing putative dsDNA hydrolytic catalysis. One of the key points to be addressed in this study is the stereochemistry around the ligating agent (e.g., **6b**) when bound to dsDNA and the conformational changes of the dsDNA which can occur upon binding. In this study the solution structure of the 1:1 complex of the dodecamer d(CGCAAATTTGCG)$_2$ with **6b** has been determined and compared to the solution structure of the same dodecamer complexed with **5c**. Solution structures were obtained by use of nuclear Overhauser effect spectroscopy (NOESY) and restrained molecular modeling (RM).

Results

^{1}H NMR Melting Study of d(CGCAAATTTGCG)$_2$. The melting temperature of a dsDNA oligomer can be estimated from the number of A·T and G·C base pairs (bp) it contains[7] (eq 1, Experimental Section). Using eq 1, the calculated melting temperature, T_m, for d(CGCA$_3$T$_3$GCG)$_2$ is 30.4 °C. By UV/vis we found a value of 31.5 °C for T_m using the method previously described.[2d] ^{1}H NMR variable temperature study on d(CGCA$_3$T$_3$GCG)$_2$ was performed between 20 and 60 °C (Figure 1) using 2,2-dimethyl-2-silapentane-*3,3,4,4,5,5-d*$_6$-5-sulfonate (DSS) as an internal reference. There is a shoulder downfield from the signals of the aromatic guanosine, G$_i$H8, protons (see Experimental Section for **Notations**) at 7.9 ppm (even at 20 °C) which increases with increasing temperature (Figure 1, marked with asterisk), while the initial G$_i$H8 composite signal (at 20 °C) decreases with increase in temperature. At 35 °C there is a partition of ca. 50% between the paired and melted guanosine aromatic signals. The thymidine methyl signals (1.2–1.7 ppm) do not undergo significant change up to 45 °C. However, above this temperature, they broaden and/or disappear in the t_1 noise.

Titration of d(CGCAAATTTGCG)$_2$ with 6b. All changes in the imino proton region (12–15 ppm) occur prior to reaching a 1:1 ratio of d(CGCA$_3$T$_3$GCG)$_2$ and **6b** when recording the ^{1}H NMR spectra in 9:1 H_2O:D_2O solvent.[6] The titration of d(CGCA$_3$T$_3$GCG)$_2$ (3.8×10^{-4} M) with **6b** was carried out in 0.25 mol equiv steps in D_2O at 21 °C (Figure 2). In contrast with the H_2O experiment, the nonexchangeable proton signals continue to change after reaching a mol ratio of 1:1 in **6b**/d(CGCA$_3$T$_3$GCG)$_2$ when titrating in D_2O (*vide infra*). In these titrations we employed mesitoate (2,4,6-trimethylbenzoate), at a 1:1 mol ratio with respect to dsDNA, as an internal standard. The mesitoate CH_3 protons resonate at 2.22 ppm (2,6-positions) and 2.24 ppm (4-position), while the aromatic protons (3,5-positions) are at 6.90 ppm. The titration was followed up to a 2.5 mol ratio of **6b** to d(CGCA$_3$T$_3$GCG)$_2$. The affected dsDNA resonances double at the 1:1 mol ratio and give line broadenings. At the 2:1 mol ratio, the resonances corresponding to the 1:1 ratio have collapsed, and one observes only one set of equivalent resonances when monitoring the thymidine methyl signals (1.2–1.7 ppm). There is a downfield shift of the aromatic adenosine signals of d(CGCA$_3$T$_3$GCG)$_2$ (Figure 2, 0–2.00 mol ratio) and an upfield shift of the pyrrole aromatic signals of **6b** (Figure 2, 1.25–2.00 mol ratio).

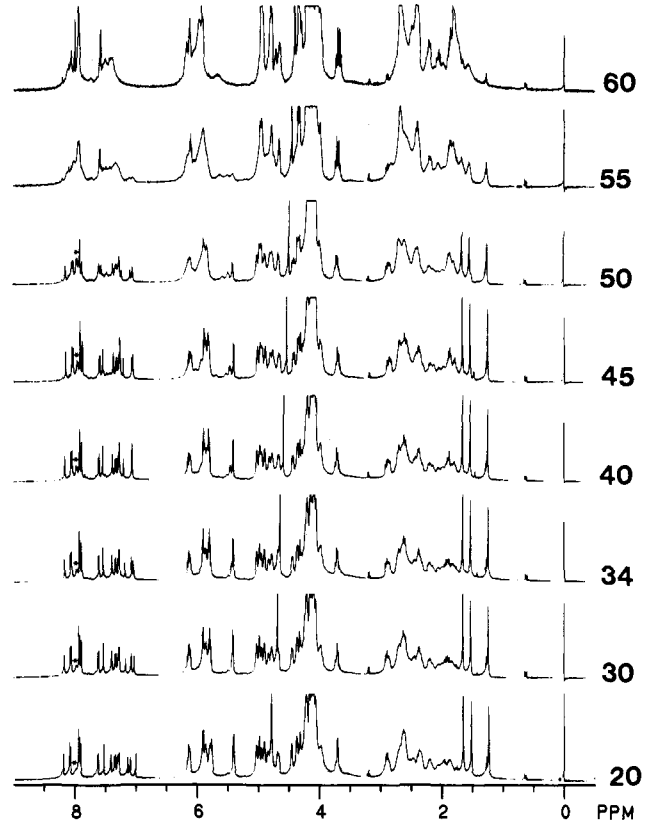

Figure 1. ^{1}H NMR melting experiment of 4×10^{-4} M d(CGCA$_3$T$_3$GCG)$_2$ (10 mM phosphate buffer, pH 7.0, 10 mM NaCl) showing spectral changes at the indicated temperatures. The terminal guanosine aromatic protons (8.0 ppm) have melted forms even at 20 °C; their resonances increase with increasing temperature (marked with asterisks).

The assignment of the resonances of 6b in D_2O (DQF-COSY, Figure S1) is shown in Table 1. These assignments were used as a lead for the assignment of the resonances of **6b** in the dsDNA:**6b** 1:1 complex. The DQF-COSY spectrum of the 1:1 complex (Figure S2-S5) shows the connectivities in the R2 and R3 propylamine and tren-polyamine substituents; their chemical shifts are summarized in Table 1. The H2, H4, and H6 pyrrole resonances of **6b** (Chart 2a) are found in the 6.5–6.8 ppm region. They give NOEs with the aromatic adenosine $A_{-7}A_{-8}$H2 protons (Chart 2b) of the (–) strand and with the sugar A_{-8}H1′ proton. The H1, H3, and H5 resonances of **6b** were assigned using their intramolecular interactions with the CH_2^n(i) methylenes of the central hydrocarbon linker and with the CH_3^{R1} group of the acetamide substituent (Figures 3 and 4). The assignment of the **6b** resonances were confirmed by the NOE enhancements in the NOESY spectrum (Figures 3, 4, 5, S6, and S7).

(7) (a) Itakura, K.; Rossi, J. I.; Wallace, R. B. *Ann. Rev. Biochem.* **1984**, *53*, 323; (b) Bolton, E. J.; McCarthy, B. J. *Proc. Natl. Acad. Sci. U.S.A.* **1962**, *48*, 1390.

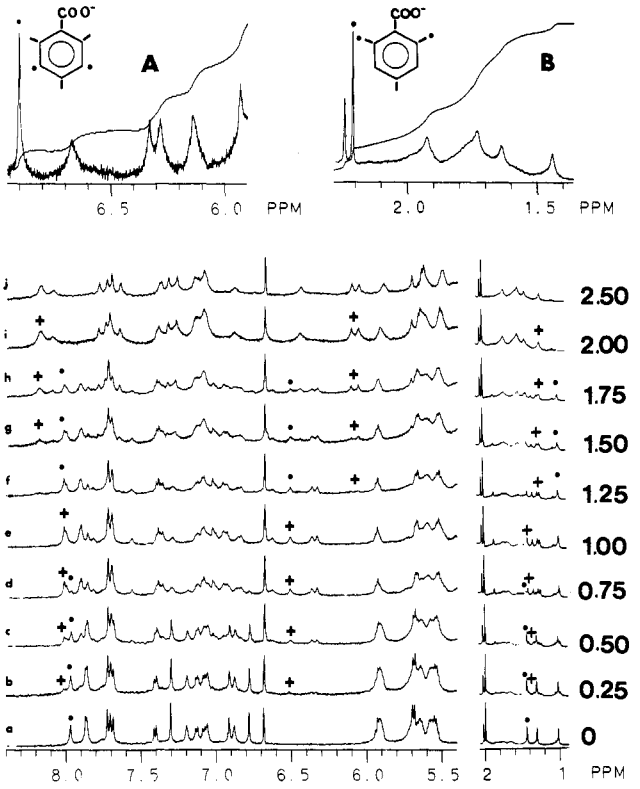

Figure 2. ^{1}H NMR titration of 3.8×10^{-4} M d(CGCA$_3$T$_3$GCG)$_2$ in D_2O (10 mM phosphate buffer, pH 7.0, 10 mM NaCl, 3.8×10^{-4} M mesitoate) with tren-microgonotropen-b (**6b**) at the indicated mole ratios of **6b**/dsDNA. The titration was followed by the disappearance of the resonances marked with asterisks and the appearance of the resonances marked with (+) signs. Insets A and B (**6b**/dsDNA = 2:1) show that the 3,5 aromatic protons of mesitoate (internal standard) integrate 1:1 with each of the pyrrole protons of **6b** (inset A) and the 2,6 CH_3's of mesitoate integrate 1:1 with each of the T_7, T_8, and T_9 equivalent CH_3 protons of the (+) and (–) strands (inset B).

Table 1. ^{1}H Chemical Shifts for 6b, Free and in the 1:1 Complex with d(CGCA$_3$T$_3$GCG)$_2$ in D_2O[a]

residue	proton	d(CGCA$_3$T$_3$GCG)$_2$:**6b**	**6b**	$\Delta\delta$[b]
pyrrole	H1	7.07	7.18	–0.11
pyrrole	H3	7.24	7.01	0.23
pyrrole	H5	7.26	7.06	0.20
pyrrole	H2	6.63	6.70	–0.07
pyrrole	H4	6.74	6.74	0.00
pyrrole	H6	6.57	6.71	–0.14
R1	methyl	2.08	1.98	0.10
R3	methyl	2.87	2.63	0.24
R4	methyl	3.97	3.76	0.21
R5	methyl	3.97	3.76	0.21
CH_2^{R2}	(1)	2.36	2.70	–0.34
CH_2^{R2}	(2)	2.62	2.92	–0.30
CH_2^{R2}	(1′)	3.01	2.94	0.07
CH_2^{R2}	(2′)	2.77	2.68	0.09
CH_2R^3	(1)	3.12	3.33	–0.21
CH_2^{R3}	(2)	1.87	1.90	–0.03
CH_2^{R3}	(3)	2.03	2.88	–0.85
CH_2^n	(1)	5.41	4.18	1.23
CH_2^n	(2)	1.76	1.73	0.03
CH_2^n	(3)	2.16	1.60	0.56
CH_2^n	(4)	3.14	2.85	0.29

[a] δ in ppm relative to TSP at 10 °C; [dsDNA] = 2.5×10^{-3} M (10 mM phosphate buffer, pH 7.0, 10 mM NaCl). [b] $\delta_{complex} - \delta_{free}$.

Assignment of ^{1}H Chemical Shifts of d(CGCAAATTTGCG)$_2$ in the 1:1 Complex with 6b. The finding of two sets of Watson–Crick G≡C and A=T resonances[6] and two sets of thymidine CH_3 resonances at the 1:1 mol ratio of **6b**/d(CGCA$_3$T$_3$GCG)$_2$ is indicative of an asymmetric, monomeric binding of the ligand to the DNA molecule, as was found in the case of the d(CGCA$_3$T$_3$GCG)$_2$:**5c** complex.[2e] The aromatic base protons H8 and H6 of the purines and pyrimidines were assigned (see Experimental Section) through their interactions with the (n–1)H2″ sugar protons and their own H1′ protons. The thymidine CH_3 protons were assigned through the interactions with their own base protons (H6) and through their interactions with the neighboring thymidine CH_3's or A_6H8 and A_{-7}H8 protons for the (+) and for the (–) strand, respectively (Figure 4 and Table 2). The sugar proton resonances were assigned from the DQF-COSY and the NOESY spectra of the complex which complement each other. Expansion of the NOESY spectrum in the (1.1–3.0) × (6.7–8.5) ppm region (Figure 4) shows the general pattern of NOESY interactions of H6/8-H2′2″, H6/8-T_iCH_3, and T_iCH_3-$T_{i+1}CH_3$ used for the assignment of sugar H2′2″ proton resonances (Table 3). A good point to initiate assignments of the dsDNA resonances is at the signals of $T_7T_{-6}CH_3$. This procedure was used in the case of free d(CGCA$_3$T$_3$GCG)$_2$ and the d(CGCA$_3$T$_3$GCG)$_2$:**5c** complex.[2e] The $T_7T_{-6}CH_3$ signals were used for the assignment of A_6A_{-7}H8, $T_7T_8T_9$H6, and $T_{-4}T_{-5}T_{-6}$H6 proton resonances (Figure 4). Here and elsewhere[2e] we use the convention that the (+) strand is the binding site side and the (–) strand is the complementary DNA strand. The remaining aromatic resonances were assigned using the known resonances of cytidine H6/5 (DQF-COSY, Figure S2) which give strong intraresidual NOEs (Figure 3) and using the interactions between two adjacent $A_{n-1}A_n$H8 protons (8.05 and 8.25 ppm). We also used the proven fact that **6b** binds into the minor groove at A + T-rich regions.[3]

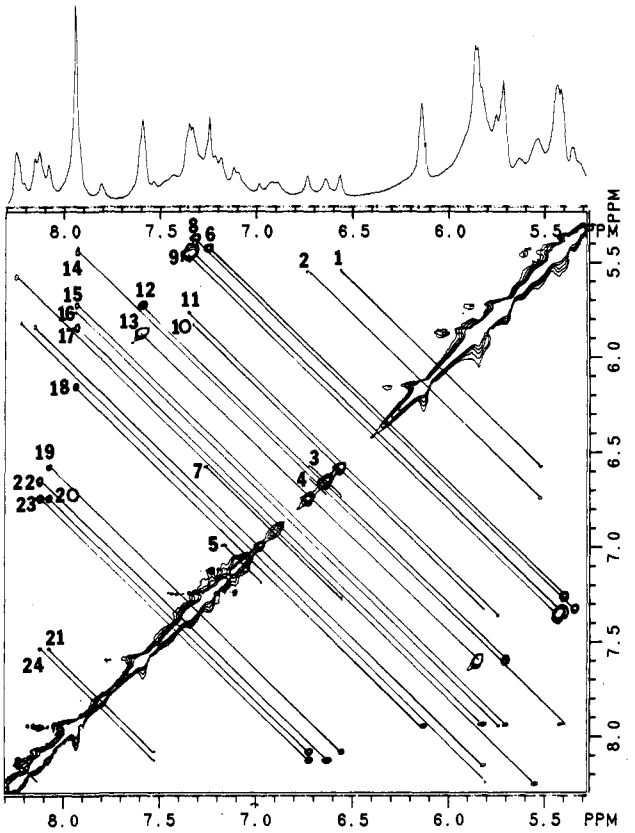

Figure 3. Expansion of the NOESY spectrum in the (5.3–8.3) × (5.3–8.3) ppm region of the 1:1 complex of d(CGCA$_3$T$_3$GCG)$_2$, 2.5×10^{-3} M with **6b** in 99.96% D_2O containing 10 mM NaCl and 10 mM phosphate buffer, pH 7.0 at 10 °C (τ_m = 180 ms): 1. H6-A_{-8}H1′, 2. H4-A_{-8}H1′, 3. H4-H6, 4. H4-H2, 5. A_4H2-A_5H2, 6. H3-CH_2^n(1), 7. H6-H5, 8. C_{-2}H6-C_{-2}H5, 9. C_{11}H6-C_{11}H5, C_3H6-C_3H5, 10. C_{11}H6-G_{10}H1′, 11. C_3H6-C_3H1′, 12. C_1H6-C_1H1′, 13. C_1H6-C_1H5, 14. G_{12}H8-C_{11}H5, 15. G_2H8-C_1H1′, 16. G_{-3}H8-T_{-4}H1′, 17. G_2H8-G_2H1′, 18. G_{12}H8-G_{12}H1′, 19. A_{-8}H2-H6, 20. A_{-8}H2-H4, 21. A_{-9}H2-A_{-8}H2, 22. A_{-7}H2-H2, 23. A_{-7}H2-H4, 24. A_{-9}H2-A_{-7}H2, 25. A_{-9}H8-A_{-9}H1′, A_6H8-A_6H1′, 26. A_4H8-A_4H1′, 27. A_5H8-A_5H1′, and 28. A_{-8}H8-A_{-9}H8, A_6H8-A_6H8.

Table 2. Comparison of the Sequential NOEs for (a) $d(CGCA_3T_GCG)_2$[2d] and (b) the 1:1 Complex of $d(CGCA_3T_3GCG)_2$ with **6b**

a. (±) strand:	C_1	G_2	C_3	A_4	A_5	A_6	T_7	T_8	T_9	G_{10}	C_{11}	G_{12}
H6/8 - CH_3						O	O	O	O			
H6/8 - H1'	O		O			O		O	O			
H6/8 - H2"	O		O	O		O	O	O	O	O	O	O
CH_3 - CH_3						O		O				
H6 - H6						O		O	O	O		

b. (+) strand:	C_1	G_2	C_3	A_4	A_5	A_6	T_7	T_8	T_9	G_{10}	C_{11}	G_{12}
H6/8 - CH_3/H5/6/8						O	O	O	O		O	O
H6/8/5 - H1'	O		O							O		O
H6/6/CH_3 - H2"	O		O	O		O		O	O	O		O
H6/8 - H3'											O	
H2/CH_3 - H2/CH_3				O		O		O				

b. (−) strand:	C_{-12}	G_{-11}	C_{-10}	A_{-9}	A_{-8}	A_{-7}	T_{-6}	T_{-5}	T_{-4}	G_{-3}	C_{-2}	G_{-1}
H6/8 – CH_3/H5/6/8				O		O	O	O	O		O	O
H6/8 - H1'				O					O			
H6/8/CH_3 - H2"		O		O		O	O				O	O
H6/8 - H3'											O	
H2/CH_3 - H2/CH_3				O		O	O	O	O			

We saw NOE enhancements between $A_{-8}H8$ and $A_{-9}H8$ and also weak enhancements between A_5H8 and A_6H8. Both enhancements were used for the dsDNA sequential assignment. The guanosine H8 resonances (7.8–8.0 ppm) were used to define the $C_1G_2G_{12}H1'$ and $T_{-4}H1'$ resonances (Figure 3). We did not see NOE buildups between $G_{10}H8$ and any of the H3′ or H5′5″ protons and no NOEs between adenosine H8 and H5′5″ protons. Defining the position of A_6H1' is important in the intracomplex interactions (*vide infra*). We found weak NOEs between A_6H8 and A_6H1' (Figure 3). The crowded region of H4′ and H5′5″ was resolved (where possible) using their NOEs with H1′ protons (Figure S6 and Table 3).

Intracomplex Interactions of d(CGCAAATTTGCG)$_2$ and 6b. Tren-microgonotropen-b (**6b**) binds into the A + T-rich region of the minor groove of $d(CGCA_3T_3GCG)_2$ in 1:1 and noncooperative 2:1 mol ratios. These complexations also involve one G·C bp (*vide supra*). Expansion of the NOESY spectrum in the (5.3–8.3) × (5.3–8.3) ppm region reveals strong NOE interactions between the H2, H4, and H6 pyrrole protons and the $A_{-8}H2$ and $A_{-7}H2$ protons as well as a small NOE for H4 with the sugar $A_{-8}H1'$ proton (Figures 3 and S6). The acetamido CH_3^{R1} methyl protons of **6b** give NOEs with $T_{-4}H6$ and A_6H1' (Figures 4 and 5) defining the orientation of the **6b** molecule in the minor groove. The dimethylpropylamino substituent, R3, approaches the G_{10} residue, defined by the NOE buildup between the CH_3^{R3} and $G_{10}H1'$ protons (Figure 5). The tren polyamino substituent of the central pyrrole ring of **6b** strongly interacts with the sugar protons of T_8 and T_9. We saw NOEs between $CH_2^n(2)$ and T_8T_9-H3′, between $CH_2^n(3)$ and T_9H3' (Figure 5), and between $CH_2^n(4)$ and T_8H5'' (Figure S7). Other intracomplex interactions were seen between CH_3^{R5} and T_9H4' (Figure S6) and between H5 and $A_{-8}H2''$ (Figure 4). An interresidual NOE was also seen between T_7H5'' and A_6H2 (Figure S8). No NOEs were detected between the R2 polyamino substituent of **6b** and $d(CGCA_3T_3GCG)_2$. However, the NOE buildup between $CH_2^n(4)$ and $CH_2^{R2}(2')$ protons (Figures 6 and S7) defined the position of this part of the R2 polyamine substituent of **6b** with regard to the dsDNA molecule {note that the position of the CH_2^n chain was already defined from their NOEs with $d(CGCA_3T_3GCG)_2$; *vide supra*}. A survey of the sequential NOEs for the DNA selected protons in the ligated dsDNA is shown in Table 2.

Induced chemical shift differences ($\Delta\delta$) were observed in certain proton resonances (Figure 7) due to the minor groove binding. This is primarily due to the ring current effect from both the dsDNA and the tripyrrole peptide. The $\Delta\delta$ extends beyond the binding site due to distortion of the dsDNA upon binding. With the exception of the T_8H5'' {$\Delta\delta$ = –0.8 ppm, Figure 7}, the differences are greater for the H1′ protons (minor groove pointers) than for any other selected protons. The increase in $\Delta\delta$ follows the order H2′ < H6/8 < H3′ < H2″ ≅ H5′ < H1′. The aromatic pyrrole protons, H3 and H5, give upfield shifts upon binding ($\Delta\delta$ = 0.2 ppm), while H1, H2 and H6 give downfield shifts ($\Delta\delta$ = –0.1 ppm) (Table 1). All the CH_3 groups of R1, R3, R4, and R5 give upfield shifts ($\Delta\delta$ = 0.1–0.2 ppm). Small downfield shifts were seen in the case of $CH_2^{R2}(1')$, $CH_2^{R3}(1)$, $CH_2^{R3}(2)$ ($\Delta\delta \leq -0.1$ ppm) and small upfield shifts in the case of $CH_2^{R2}(2')$ and $CH_2^n(2')$ ($\Delta\delta$ = 0.2 ppm). Large upfield shifts are exhibited by the hydrocarbon linker methylene resonances ($\Delta\delta$ = 0.3–1.2

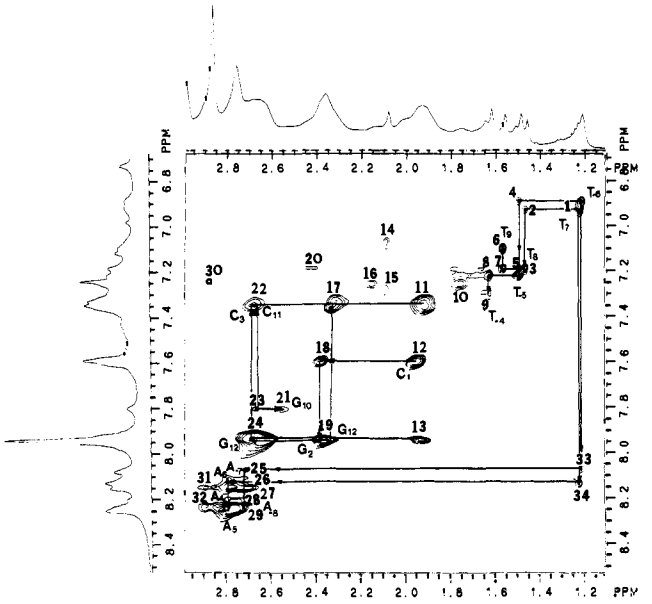

Figure 4. Expansion of the NOESY spectrum in the (6.7–8.5) × (1.1–3.0) ppm region of the 1:1 complex of $d(CGCA_3T_3GCG)_2$, 2.5 × 10^{-3} M with **6b** in 99.96% D_2O containing 10 mM NaCl and 10 mM phosphate buffer, pH 7.0 at 10 °C (τ_m = 180 ms): 1. T_7H6-T_7CH_3, $T_{-6}H6$-$T_{-6}CH_3$, 2. T_7H6-T_8CH_3, 3. T_8H6-T_8CH_3, 4. $T_{-6}H6$-$T_{-5}CH_3$, 5. $T_{-5}H6$-$T_{-5}CH_3$, 6. T_9H6-T_9CH_3, 7. T_8H6-T_9CH_3, 8. $T_{-5}H6$-$T_{-4}CH_3$, 9. $T_{-4}H6$-$T_{-4}CH_3$, 10. H5-$CH_2^n(2)$, 11. $C_3C_{11}H6$-$C_3C_{11}H2'$, 12. C_1H6-C_1H2', 13. $G_2G_{12}H8$-$C_1C_{11}H2'$, 14. H_1-CH_3^{R1}, 15. $T_{-4}H6$-CH_3^{R1}, 16. H3-$CH_2^n(3)$, 17. $C_3C_{11}H6$-$C_3C_{11}H2''$, 18. C_1H6-C_1H2'', 19. G_2G_{12}-$H8$-$C_1C_{11}H2''$, 20. T_8H6-T_7H2'', 21. $G_{10}H8$-$G_{10}H2'$, 22. $C_3C_{11}6$-$G_2G_{10}H2''$, 23. $G_{10}H8$-$G_{10}H2''$, 24. $G_2G_{12}G_{-3}H6$-$G_2G_{12}G_{-3}H2''$, 25. $A_{-7}H8$-$A_{-7}H2'$, 26. A_6H8-$A_6H2'2''$, 27. $A_{-9}H8$-$A_{-9}H2'$, 28. A_4H8-$A_4H2'2''$, 29. A_5H8-$A_5H2'2''$, 30. H5-$A_{-8}H2''$, 31. $A_{-9}H8$-$A_{-9}H2'2''$, 32. $A_{-8}H8$-$A_{-8}H2'2''$, 33. $A_{-7}H8$-$T_{-6}CH_3$, and 34. A_6H8-T_7CH_3.

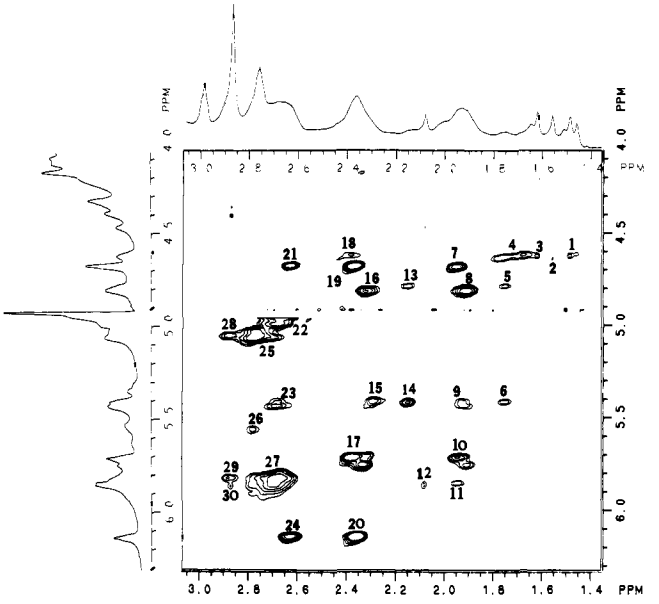

Figure 5. Expansion of the NOESY spectrum in the (1.4–3.1) × (4.0–6.3) ppm region of the 1:1 complex of $d(CGCA_3T_3GCG)_2$, 2.5 × 10^{-3} M with **6b** in 99.96% D_2O containing 10 mM NaCl and 10 mM phosphate buffer, pH 7.0 at 10 °C (τ_m = 180 ms). 1. $T_{-5}T_8CH_3$-$T_{-5}T_8H3'$, 2. T_9CH_3-T_9H3', 3. $T_{-4}CH_3$-$T_{-4}H3'$, 4. $CH_2^n(2)$-T_8H3', 5. $CH_2^n(2)$-T_9-$H3'$, 6. $CH_2^n(1)$-$CH_2^n(2)$, 7. C_1H2'-C_1H3', 8. $C_1C_{11}H2'$-$C_1C_{11}H3'$, 9. $C_3C_{11}H2'$-$C_3C_{11}H5$, 10. $C_1C_3C_{11}H2'$-$C_1C_3C_{11}H1'$, 11. C_1H2'-C_1H5, 12. CH_3^{R1}-A_6H1', 13. $CH_2^n(3)$-T_9H3', 14. $CH_2^n(3)$-$CH_2^n(1)$, 15. C_3C_{11}-$H2''$-$C_3C_{11}H5$, 16. $C_3C_{11}H2''$-$C_3C_{11}H3'$, 17. $C_3C_{11}H2''$-$C_3C_{11}H1'$, 18. $T_7T_{-5}H2''$-$T_7T_{-5}H3'$, 19. $G_{12}H2'$-$G_{12}H3'$, 20. $G_{12}H2'$-$G_{12}H1'$, 21. G_{12}-$H2''$-$G_{12}H3'$, 22. $G_2G_{10}H2''$-$G_2G_{10}H3'$, 23. $C_3C_{11}H5$-$G_2G_{10}H2''$, 24. $G_{12}H2''$-$G_{12}H1'$, 25. $A_4A_5A_6H3'$-$A_4A_5A_6H2'2''$, 26. $A_5A_{-8}H1'$-A_5A_{-8}-$H2''$, 27. $A_4A_6G_{10}G_2H1'$-$A_4A_6G_{10}G_2H2'2''$, 28. $A_{-9}A_{-8}H1'$-$A_{-9}A_{-8}$-$H2''$, 29. $A_{-9}H2''$-$A_{-9}H1'$, and 30. CH_3^{R3}-$G_{10}H1'$.

ppm), the highest ($\Delta\delta$ = 1.2 ppm) being at $CH_2^n(1)$. Large downfield shifts were seen in the case of $CH_2^{R3}(3)$ ($\Delta\delta$ = –0.8 ppm) and in the cases of $CH_2^{R2}(1)$ and $CH_2^{R2}(2)$ ($\Delta\delta$ = –0.3 ppm). These are due to their adjacent protonated amines which are involved in hydrogen bonding to phosphates.

Sugar Puckerings of $d(CGCAAATTTGCG)_2$. From the DQF-COSY spectrum of the $d(CGCA_3T_3GCG)_2$:**6b** complex (Figures S2-S5), coupling constants can be estimated, and, therefore, some sugar residues can be characterized in terms of their vicinal proton dihedral angles. In terms of sugar puckering, the DNA's backbone conformation is dictated by the glycosidic torsion angle defined by C5′–C4′–C3′–O3′. The exact ^3J coupling constants involving H3′ are hard to determine due to their passive coupling including phosphorus.[8] However, they can be qualitatively constrained into restricted ranges from the corresponding cross peaks intensities.[8] Cross peaks between H3′–H2″ and H3′–H4′ were weak or nonexistent in the DQF-COSY spectrum of the 1:1 complex (Figure S2) except for some terminal base pairs. These very small coupling constants are indicative of the presence of the B-form of dsDNA.[8] Since the sugar conformation can be determined from the NOESY-derived distance data, the coupling constants estimated from the DQF-COSY complements the NOESY/RM characterization of the complexed dsDNA. In the cases of the well resolved H1′–H2″ and H1′–H2′ cross peaks, sugar coupling constants were estimated for G_{10}, G_{12}, C_1, C_3, and C_{11} to be 3–5 Hz and 1.5 Hz for A_4 and A_6 (Figures S3–S5). In all cases $^3J_{H1'-H2'} > {}^3J_{H1'-H2''}$. This limits the deoxyribose pseudorotational phase angles (P) to 90°–190°.[8] In the case of the terminal base pairs C_1, C_3, and G_{12}, the coupling constants for H3′–H4′ were 3–5 Hz, while for the binding site residue T_9/T_{-4}, 2.5 Hz, placing them close to P = 126° (H1′-exo) and P = 140°–162° (H2′-endo), respectively. No other cross peaks could be seen and/or resolved.

Table 3. ^1H Chemical Shifts for $d(CGCA_3T_3GCG)_2$ in the 1:1 Complex with **6b** in D_2O[a]

base	H1′	H2′	H2″	H3′	H4′	H5′	H5″	H6/8	H2/5/CH_3
					(+) Strand				
5′-C_1	5.71	1.95	2.37	4.68	4.04	4.03	3.70	7.60	5.82
G_2	5.84	2.64	2.68	4.94	4.33	4.40	4.35	7.94	
C_3	5.75	1.90	2.33	4.82	4.18	4.18	4.12	7.39	5.42
A_4	5.81	2.74	2.80	5.06	4.38	4.47	4.22	8.20	7.18
A_5	5.55	2.72	2.78	5.03	nd[b]	4.46	4.36	8.25	6.98
A_6	5.84	2.68	2.77	5.06	4.22	4.40	4.22	8.13	7.46
T_7	5.36	1.97	2.41	4.62	nd	4.02	3.88	6.93	1.23
T_8	5.64	2.00	2.31	4.63	3.70	3.88	3.35	7.18	1.46
T_9	5.42	1.98	2.30	4.78	4.10	4.20	4.10	7.11	1.56
G_{10}	5.84	2.55	2.66	4.98	4.01	4.35	4.12	7.80	
C_{11}	5.70	1.93	2.33	4.83	4.03	4.18	4.13	7.36	5.41
G_{12}	6.15	2.36	2.62	4.67	4.18	4.17	4.06	7.95	
					(–) Strand				
5′-C_{-12}	5.71	1.95	2.37	4.68	4.04	3.98	3.70	7.58	5.82
G_{-11}	5.84	2.64	2.68	4.94	4.33	4.40	4.35	7.94	
C_{-10}	5.75	1.90	2.33	4.82	4.18	4.18	4.12	7.39	5.42
A_{-9}	5.81	2.79	2.89	5.06	nd	4.47	4.22	8.15	7.53
A_{-8}	5.52	2.78	2.89	5.08	4.22	4.46	4.36	8.23	8.08
A_{-7}	5.86	2.71	2.81	5.05	nd	4.40	4.22	8.08	8.12
T_{-6}	5.70	1.97	2.41	4.64	nd	4.15	3.92	6.87	1.21
T_{-5}	6.17	2.00	2.40	4.62	3.70	4.00	3.85	7.22	1.48
T_{-4}	5.75	1.98	2.42	4.78	4.10	4.15	4.10	7.28	1.62
G_{-3}	5.78	2.36	2.66	4.97	4.01	4.10	3.98	7.92	
C_{-2}	5.70	1.93	2.32	4.83	4.03	4.18	4.13	7.36	5.35
G_{-1}	6.15	2.36	2.62	4.67	4.18	4.17	4.06	7.95	

[a] δ in ppm relative to TSP at 10 °C; [dsDNA] = 2.5 × 10^{-3} M (10 mM phosphate buffer pH 7.0, 10 mM NaCl). The Watson–Crick imino protons (recorded in H_2O)[6] are in the range A=T 13.5–14.2 and G≡C 12.5–13.1 ppm. [b] Not determined.

(8) Kim, S.-G.; Lin, L.-J.; Reid, B. R. *Biochemistry* **1992**, *31*, 3564.

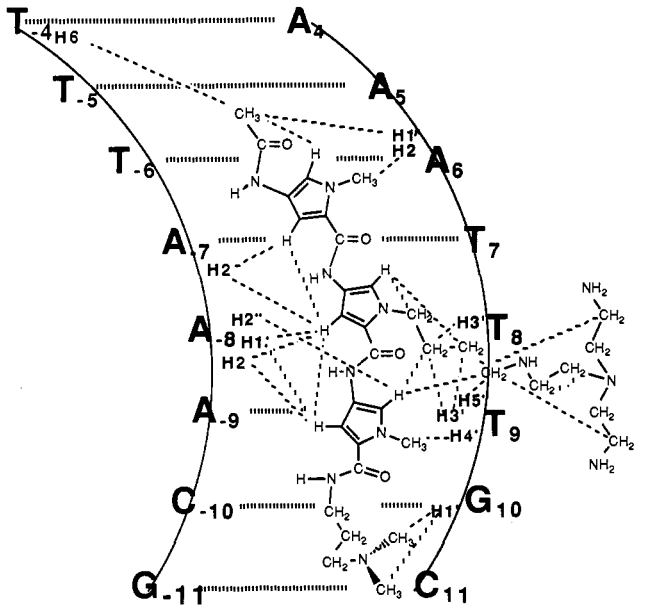

Figure 6. Schematic representation of the dsDNA-**6b** intracomplex and **6b** intramolecular NOE interactions (represented by broken lines) in the 1:1 complex of $d(CGCA_3T_3GCG)_2$ at 2.5 mM with **6b** in 99.96% D_2O containing 10 mM NaCl and 10 mM phosphate buffer, pH 7.0 at 10 °C. The sugar protons are labeled with prime and double prime (see Experimental Section) and placed next to the residue they belong. The aromatic A_{-7} and $A_{-8}H2$ protons give NOE interactions with the aromatic pyrrole protons of **6b**, defining the position of the tripyrrole peptide moiety in the A+T-rich region.

Distance Calculations and Restrained Molecular Modeling Refinements. For the 1:1 complex of the dodecamer $d(CGCA_3T_3GCG)_2$ and **6b**, 155 intramolecular interactions were found for both NMR-nonequivalent strands. Of these, 17 were used in refining the DNA distances of the previously determined solution structure of $d(CGCA_3T_3GCG)_2$[2e] (Table 4). These intramolecular interactions represent the only well separated cross peaks (Table 2). In addition, 17 interactions between **6b** and the dsDNA and intramolecular **6b** interactions were used for docking (Figure 6; Table 4). The same minimization procedure used previously[2e] was employed to obtain the most probable solution structure of the 1:1 complex of **6b** with $d(CGCA_3T_3GCG)_2$ (Figure 8). All deviations in the refined structure from the calculated NOE distances were less than 0.6 Å (Table 4). The ROESY spectrum (Figure S9) confirms most of the NOESY enhancements.

Comparison of solution structures of $d(CGCA_3T_3GCG)_2$[2e] and the $d(CGCA_3T_3GCG)_2$:**6b** complex shows that the minor groove widens considerably between the T_{-4} to T_8 and T_{-5} to T_9 phosphates (3–4 Å, respectively) upon complexation of **6b**. The ligand binds 7.3–9.0 and 5.5–6.4 Å from the (–) and (+) strands, respectively, when examining the regions from T_{-4} to T_{-6} and G_{10} to T_8 (distances from the pyrrole nitrogens to $P_{-4}P_{-5}P_{-6}$ and $P_8P_9P_{10}$, respectively; Experimental Section). In addition, the **6b** complexed dodecamer lengthens 1 Å relative to the solution structure of the dodecamer[2e] as is evidenced by the unit height (34.93 Å/repeat). This is due to a combination of a relatively unwound helix (turn angle = 35.90°/bp), a large axial rise (3.50 Å/bp), and a fairly large helical rise (10.03 bp/repeat). The angle of the bend (α; Figure 9) in the helical axis of the solution structure of $d(CGCA_3T_3GCG)_2$ complexed with **6b** (22.2°) is more than twice the same angle for the crystal (10.8°) and only 0.8° greater than the solution (21.4°) structure of the $d(CGCA_3T_3GCG)_2$ alone.[2e] In the solution structure, the molecular contact surface area between $d(CGCA_3T_3GCG)_2$ and **6b** is 518 Å^2.

Dynamics of Ligand Exchange. The signals of the H2, H4, and H6 resonances of **6b** exhibit different line broadenings ($\Delta\nu_{1/2}$ = 14, 15, and 10 Hz, respectively) when in the 1:1 complex with $d(CGCA_3T_3GCG)_2$ (Figure 3). This is in accord with minor groove binding.[9] As previously discussed[2e] the broadening could be due to the relatively slow exchange of **6b** between two equivalent binding sites and/or to a fast sliding motion in the minor groove. Exchanges between two equivalent binding sites have been proposed for dsDNA complexes of distamycin[5] and netropsin.[10a,b] If we consider that the exchange is governed by a "flip-flop" mechanism[5] (Scheme 1), not excluding the possible existence of a fast sliding motion of **6b** in the minor groove, the rate of exchange can be calculated (Experimental Section). In studying the identical line shapes of the diagonal and cross peaks, the rate of exchange for this process was found to be 1.3 ± 0.2 s^{-1} (10 °C, Experimental Section) corresponding to an activation energy (ΔG^*) of ~17 kcal/mol. The association constant of **6b** with A_3T_3 sites {e.g., $d(GGCGCA_3T_3GGCGG)/d(CCGCCA_3T_3GCGCC)$} has been determined[3] to be 8×10^8 M^{-1}. From this information, dissociation of **6b** from the hexadecamer is much slower than association, and, therefore, one can consider the rate of exchange equal to the off-rate ($k_{ex} \cong k_{off}$). Here, and elsewhere,[2e] we consider these values as estimates, and their determination does not include studies beyond our goal of cross relaxations contributing to the peak intensities and the mixing time profile.[12]

Table 4. Experimental (NOESY) and Refined (Molecular Modeling) Distances for the 1:1 Complex of $d(CGCA_3T_3GCG)_2$ with 6b in D_2O[a,d]

Distances Involving Only $d(CGCA_3T_3GCG)_2$ Protons

		H1′	H2′	H5′	H6/8	$CH_3/H_5/H2^*$
G_2	H8	3.9[b](4.0)				
C3	H6	4.1(4.0)				
A_4	H8	4.9(4.3)				
A_5	H8	3.9(3.9)				
A_6	H8					4.1[b](4.1)
A_6	H2			3.4[c](3.9)		
T_8	H6		4.3[b](4.2)			3.8[c](3.8)
T_8	CH_3				4.3[b](4.4)	
G_{12}	H8	3.7(3.8)	4.9[b](4.8)			4.0[b](4.2)
T_{-5}	H6					3.8[c](3.8)
T_{-6}	H6					4.4[c](4.4)
A_{-7}	H8					4.3[c](4.3)
A_{-8}	H2					4.7*[c](4.6)
A_{-9}	H8	4.2(4.1)				

b. Distances Involving $d(CGCA_3T_3GCG)_2$ and **6b** Protons

H2-A_{-7}H2 3.4(3.4); H4-A_{-7}H2 3.7(3.7); H4-A_{-8}H1′ 4.0(4.3); H4-A_{-8}H2 3.6(3.6); H6-A_{-8}H1′ 4.0(3.8); H6-A_{-8}H2 3.8(3.8); CH_3^{R1}-A_6H1′ 4.2(4.1); CH_2^{R1}-T_{-4}H6 4.0(4.5); $CH_2^n(3)$-T_9H3′ 3.6(4.0); $CH_2^n(2)$-T9H3′ 3.8(3.8); CH_3^{R3}-G_{10}H1′ 4.8(4.8); H1-CH_3^{R1} 3.8(4.2); H3-$CH_2^n(1)$ 3.0(3.0); H3-$CH_2^n(3)$ 3.8(4.4); H5-$CH_2^n(2)$ 3.3(3.8); $CH_2^n(4)$-$CH_2^{R2}(2)$ 4.0(4.2); $CH_2^n(4)$-$CH_2^{R2}(2')$ 4.0(4.2)

[a] In Å, with the same residue. [b] Distances with the $(n-1)$ residue. [c] Distances with the $(n+1)$ residue. Distances marked with asterisks (*) belong to the protons marked with asterisks. [d] Refined distances are in parentheses.

Discussion

Both 1:1 and 2:1 complexes of $d(CGCA_3T_3GCG)_2$ with **6b** have been observed. The solution structure of the 1:1 complex of $d(CGCA_3T_3GCG)_2$ with **6b** has been determined by 2D NMR

(9) Umemoto, K.; Sarma, M. H.; Gupta, G.; Luo, J.; Sarma, R. H. *J. Am. Chem. Soc.* **1990**, *112*, 4539.
(10) (a) Patel, D. J.; Shapiro, L. *Biochimie* **1985**, *67*, 887. (b) Patel, D. J.; Shapiro, L. *J. Biol. Chem.* **1986**, *261*, 1230. (c) Patel, D. J.; Shapiro, L.; Hare, D. *Q. Rev. Biophys.* **1987**, *20*, 35. (d) Gao, X.; Patel, D. J. *Q. Rev. Biophys.* **1989**, *22*, 93. (e) Hare, D. R.; Wemmer, D. E.; Chou, S.-H.; Drobny, G.; Reid, B. R. *J. Mol. Biol.* **1983**, *171*, 319.
(11) Saenger, W. *Principles of Nucleic Acid Structure*; Springer-Verlag: New York, 1984; p 148.
(12) Klevit, R. E.; Wemmer, D. E.; Reid, B. R. *Biochemistry* **1986**, *25*, 3296.

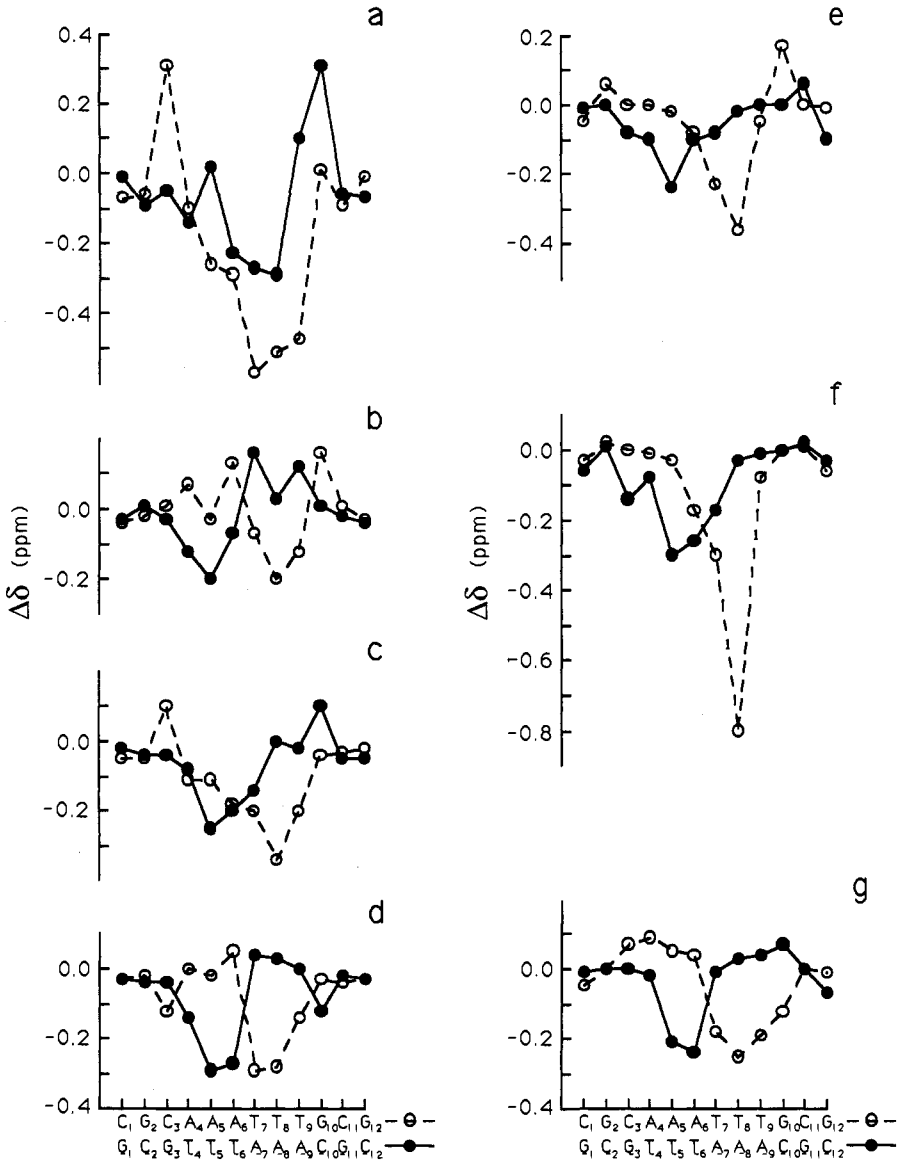

Figure 7. Induced chemical shift differences between the 1:1 complex of $d(CGCA_3T_3GCG)_2$ with **6b** and the free dsDNA *vs* the dsDNA sequence for the selected dsDNA protons: (a) H1′, (b) H2′, (c) H2″; (d) H3′, (e) H5′, (f) H5″, and (g) H6/8. $\Delta\delta = \delta_{complex} - \delta_{free\ dsDNA}$.

Scheme 1

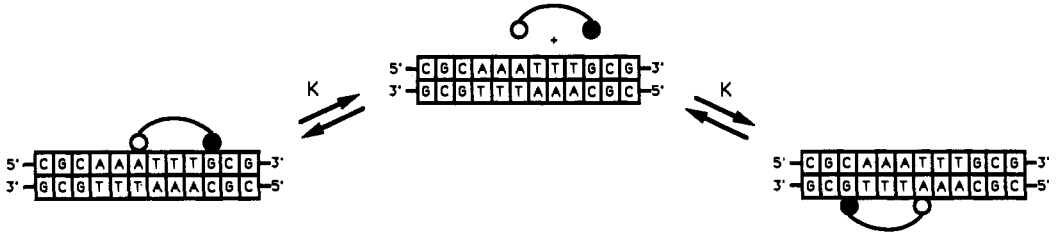

spectroscopy and restrained molecular modeling. Due to the complexity of ligation and the dynamics of **6b** in the complex with dsDNA, small populations of the free dodecamer or of dodecamer:ligand complexes other than those reported here may exist in solution.

Our NMR observation that at 35 °C the end G·C base pairs exist equally as paired and as melted forms is consistent with the spectroscopically determined T_m of 31.5 °C (Figure 1). In the aromatic guanosine resonances at 7.9 ppm, one can observe the melted form of the terminal base pairs even at 20 °C. By 10 °C melting is barely discernable. One might suppose, therefore, that binding studies should be carried out at ≤10 °C in order for the structure of $d(CGCA_3T_3GCG)_2$ to be intact. However, we found that ligation by A + T-rich minor groove binding agents such as **6b**, **5c**, or distamycin[6] is not significantly affected by the "fraying" of the end base pairs of $d(CGCA_3T_3GCG)_2$ at the temperatures of 10, 21, and 35 °C. It was found[2e,6] that microgonotropens stiffen the $d(CGCA_3T_3GCG)_2$ molecule, diminishing the percentage of the end base pairs in melted forms. The structural changes that occur at the G·C ends in the early stages of the dsDNA melting are consistent with previous studies in which a larger population of terminal base pairs were found to be melted as compared to interior base pairs.[11] The unchanged thymidines' CH_3 region between 20 and 45 °C show that, under the conditions of these experiments, $d(CGCA_3T_3GCG)_2$ maintains its base pairing in the A_3T_3 region even at 45 °C! However, to maximize

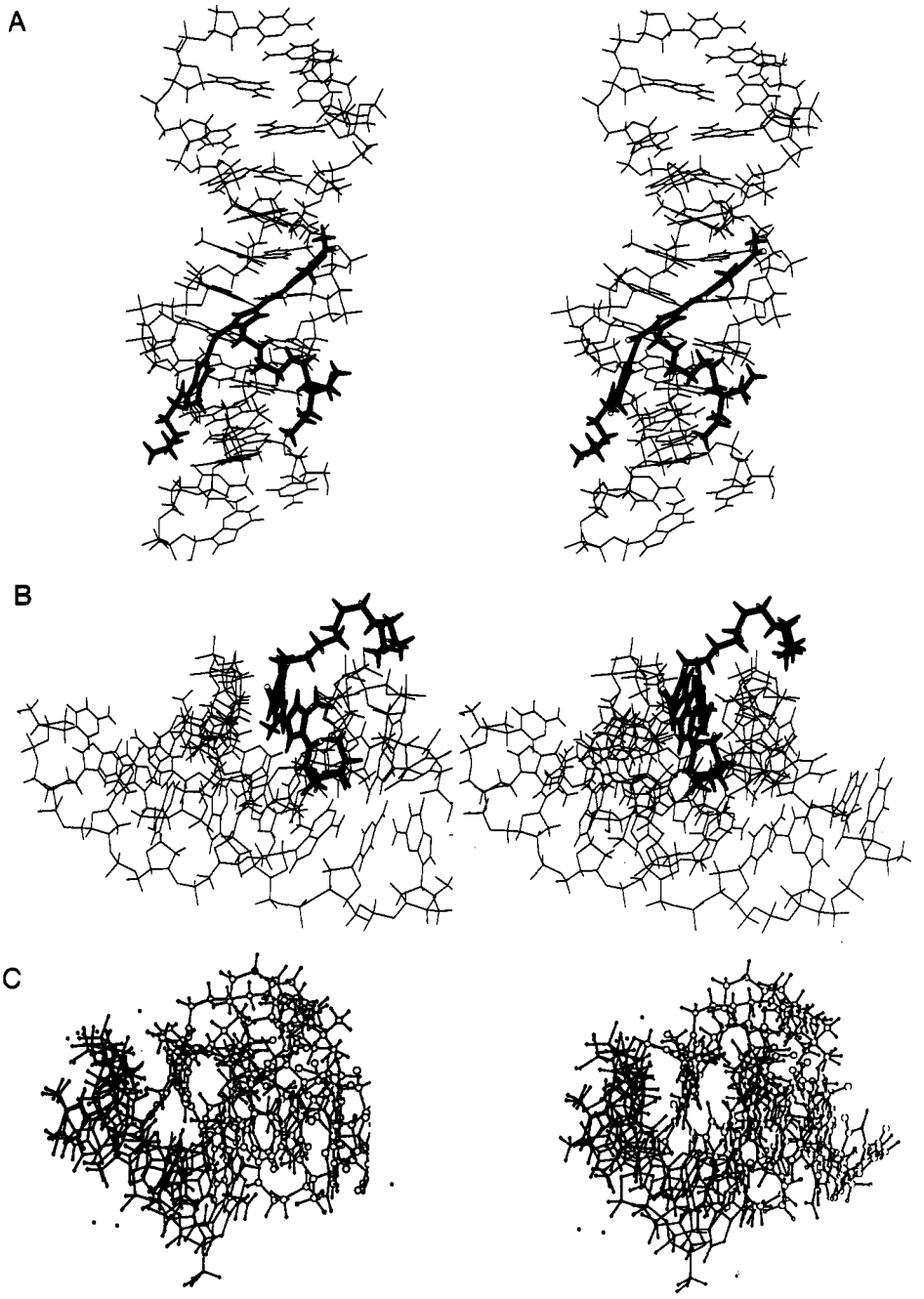

Figure 8. Stereo models of the D_2O solution structure of (a and b) the 1:1 complex of $d(CGCA_3T_3GCG)_2$ with **6b** and (c) an overlay of two structures of the 1:1 complex of $d(CGCA_3T_3GCG)_2$ with **5c**[2e] and **6b**. Figure 8b represents the view along the minor groove of the dsDNA. The "tren" substituent of **6b** is coming out of the minor groove and around the phosphate backbone.

the double stranded nature of this dodecamer {and also to slow down the tumbling and the internal motions of the 1:1 $d(CGCA_3T_3GCG)_2$:**6b** complex}, our structure determination was conducted at 10 °C.

A titration of $d(CGCA_3T_3GCG)_2$ with **6b** in H_2O/D_2O 9:1 (at 1.8×10^{-4} M of dsDNA)[6] was carried out to a ratio of 2:1 of **6b** to dsDNA. No detectable spectral changes in the imino protons' resonances were observed above a 1:1 mol ratio of **6b** to $d(CGCA_3T_3GCG)_2$ {in D_2O we could detect a 2:1 complex, *vide infra*}. The spectral changes in the imino proton region when titrating with **6b** show that **6b** targets the A + T-rich region[6] involving one G·C residue. The titration in D_2O ([dsDNA] = 3.8×10^{-4} M) was carried out to a ratio of 2.5:1 of **6b** to dsDNA. In this experiment, spectral changes in the nonexchangeable protons extended from below a 1:1 ratio to a 2:1 ratio of **6b**/$d(CGCA_3T_3GCG)_2$ (Figure 2). The doubling of the dsDNA resonances (in the D_2O experiment) below a 1:1 mol ratio is indicative of an asymmetrical type of binding {see thymidine CH_3's (1.2–1.6 ppm)} of **6b** to $d(CGCA_3T_3GCG)_2$. The collapse of these resonances to only one set at a 2:1 mol ratio is indicative of a symmetrical binding mode for two **6b** per one $d(CGCA_3T_3GCG)_2$. {In a study based on fluorescence measurements, it was found that the equilibrium constants for binding of the first and second molecule of **6b** to d(GGCGCA$_3$T$_3$GGCGG)/d(CCGCCA$_3$T$_3$GCGCC) shows slight cooperativity.[3] Using $d(CGCA_3T_3GCG)_2$ with **6b**, our ^{1}H NMR examination shows no (or undetectable) cooperativity in binding.} The inability to observe ^{1}H NMR spectral changes in the imino region above a 1:1 ratio[6] suggests that at any given time only one of two **6b** molecules resides inside the groove (Scheme 2). In the 2:1 complex there should be a fast exchange between the two molecules of **6b** when binding to $d(CGCA_3T_3GCG)_2$ such that the minor groove widens (and remains wide during the exchange of two **6b** molecules), and, as a result, spectral changes occur. On decreasing

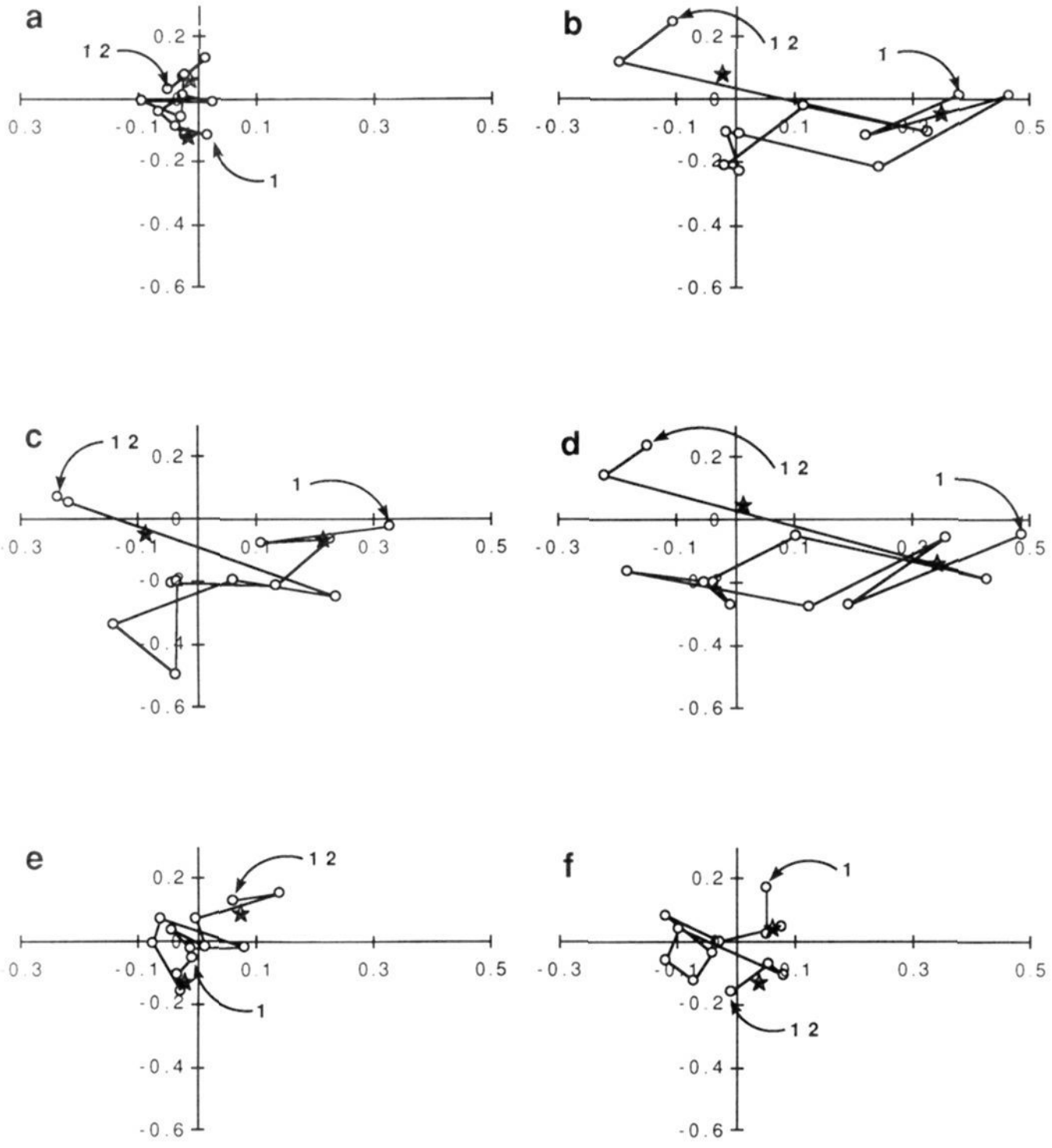

Figure 9. Normal vector plots to the mean plane of the base pairs for the d(CGCA$_3$T$_3$GCG)$_2$:**6b** complex and for previously described dodecamer structures showing the bending of the helical axes. The best DNA helix axis is perpendicular to the plane of the paper at the intersection of the *x*- and *y*-axes. The *x*- and *y*-axes are components of the changes in direction cosines of the normal vectors of the best helix axis to the best mean plane through each base pair projected onto the plane of the paper. The first and last base pairs are labeled in bold (**1** and **12**, respectively) with lines consecutively connecting the intervening base pairs. Bold star symbols (★) indicate the positions used to calculate the bending angles (α): (a) crystal structure of d(CGCA$_3$T$_3$GCG)$_2$[15b] (α = 10.8°),[2e] (b) NOE refined solution structure of d(CGCA$_3$T$_3$GCG)$_2$ (α = 21.4°),[2e] (c) NOE refined solution structure of d(CGCA$_3$T$_3$GCG)$_2$:**5c** (α = 17.2°),[2e] (d) NOE refined solution structure of d(CGCA$_3$T$_3$GCG)$_2$:**6b** (α = 22.2°), (e) crystal structure of d(CGCA$_3$T$_3$GCG)$_2$:**Dm**[15a] (α = 13.9°),[2e] and (f) NOE refined solution structure of d(CGCA$_3$T$_3$GCG)$_2$:**Dm**$_2$[5] (α = 11.3°).[2e]

Scheme 2

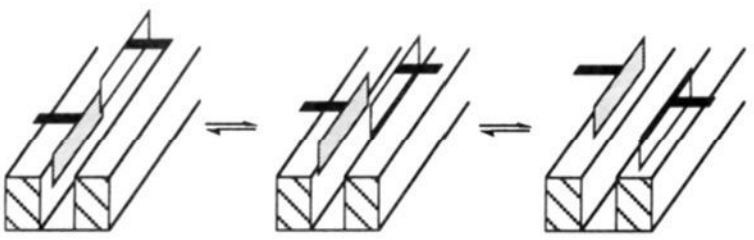

the temperature to –5 °C, the internal motions of the 2:1 complex of **6b**/d(CGCA$_3$T$_3$GCG)$_2$ ([dsDNA] = 4 × 10^{-4} M) decrease. At –5 °C broadening of the A·T resonances occurs while the G·C signals remain sharp (data not shown). It was previously shown that the 4:1 distamycin/d(CGCA$_3$T$_3$GCG)$_2$ complex[6] maintains its A·T and G·C resonance line widths when going to –10 °C. The broadening of the A·T resonances of the 2:1 complex of **6b**/d(CGCA$_3$T$_3$GCG)$_2$ at –5 °C could be due to (a) an asymmetric 2:1 rigid binding mode in which **6b** exchanges between two equivalent sites of the dsDNA or (b) a symmetrical 2:1 binding mode in which two molecules of **6b** exchange as shown in Scheme 2. The possibility of an asymmetric, rigid, 2:1 binding can be ruled out due to the existence of only one set of **6b** resonances.

The binding of the flat tripyrrole peptide portion of **6b** in the A + T-rich region of the 1:1 complex results in broadening and downfield shifting of the involved resonances.[13] Assignment of the nonexchangeable protons (Table 3) revealed two sets of DNA resonances, but only one set of **6b** resonances (Table 1). This indicates that the predominant structure involves a single type of monomeric binding.

Induced chemical shift differences reveal that the most affected protons involved in the dsDNA to **6b** interactions are H1′ and H2″ (Figure 7). These chemical shift differences also show the changes which occur at the binding site by the perturbation of the involved protons. The large chemical shift difference, $\Delta\delta$, for T$_8$H5″ indicates a strong distorsion of the dsDNA at this site. This distortion is due to the interactions between the phosphate backbone and the CH$_2^n$ hydrocarbon linker of the central pyrrole ring of **6b**, consistent with the large $\Delta\delta$ found for the CH$_2^n$ protons (Table 1). This observation is in agreement with the refined solution structure of the d(CGCA$_3$T$_3$GCG)$_2$:**6b** complex (Figure 8). The increase in the number of NOEs observed for H6/8 with

(13) Leupin, W.; Chazin, W. J.; Hyberts, S.; Denny, W. A.; Wüthrich, K. *Biochemistry* **1986**, *25*, 5902.

CH_3/H5/6/8 protons (not involved in the exchange phenomena) as compared to the free DNA[2e] can be ascribed to the stiffening of the DNA molecule at the binding site (Table 2, see H6/8 interactions with CH_3/H5/6/8) and/or to the dynamic motion of the dodecamer around a position which would bring the aromatic units of the binding site closer together as seen in the case of **5c**.[2e] By convention, we assigned this sequence to the (+) strand. The characteristics of the reduced electrophoretic mobilities on agarose gels of DNA restriction digest fragments after preincubation with **6b** suggest a distortion of DNA conformation.[3] Although the differences in the induced chemical shifts beyond the binding site are generally small, even in the case of the terminal base pairs (C_1, G_{-1} and G_{12}, C_{-12}) structural distortions occur upon binding as is evidenced by $\Delta\delta \neq 0$ (Figure 7). The significant $\Delta\delta$ for $G_{10}H2'$ enforces our observation that this proton is involved in an interaction with **6b**. A small effect on the proton resonances of the aromatic bases suggests that the binding of **6b** does not significantly affect the positions of those protons that are major groove pointers. The upfield shift of the H5′ and H5″ resonances suggests high electron density around these protons. These electron densities derive from the central tren polyamino substituent of **6b**. The acetamido function (R1, Chart 2) of **6b** affects the position of A_6H5'' to a small extent while perturbation of $G_{10}H5'$ is by the dimethylpropylamino substituent R3. These chemical shift differences suggest that, aside from the minor groove protons which experience disruption of DNA ring currents due to **6b** binding, all other affected protons are influenced by the conformational changes of the DNA which occur upon complex formation.

There are changes in base pairing and stacking as well as sugar puckering of $d(CGCA_3T_3GCG)_2$ upon formation of the $d(CGCA_3T_3GCG)_2$:**6b** complex. From the derived dihedral angles of the ribose moieties, we can state that the A·T regions of the complexed dsDNA maintain their B-conformation[8] and the terminal G·C ends do not. Instead, the G·C ends appear to exist in an intermediate B- to A-DNA form when monitored by the H3′–H4′ dihedral angles. Since the conformation of the terminal base pairs is not strictly maintained due to the dynamic "fraying" of the ends, it is not surprising that those dihedral angles do not correspond to B-DNA. This is consistent with the melting experiment in which the G·C terminal base pairs coexist in melted/paired forms even at 20 °C (Figure 1).

The $-CH_2CH_2CH_2N(CH_3)_2$ tail at the carboxyl terminus of **6b** is completely within the minor groove. This observation is consistent with the induced chemical shift differences for the R3 protons of **6b** in the complex (Table 1). The CH_3 protons of the acetamido moiety R1 are slightly deshielded while R3, R4, and R5 methyl protons are strongly deshielded due to their proximities with the phosphate backbone. A strong deshielding is observed on the first, third, and fourth methylene groups of the CH_2^n chain attached to the nitrogen of the central pyrrole ring. This suggests that these three methylenes have proximities with the dsDNA phosphates as shown by the structure of the 1:1 $d(CGCA_3T_3GCG)_2$/**6b** complex (Figure 8). The deshielding of H3 and H5 was ascribed to the pyrrole ring interactions with the phosphate ridge on the minor groove side.

Microgonotropen **6b** possesses five aliphatic amino groups: two primary, one secondary, and one tertiary in the tren substituent $\{-CH_2CH_2CH_2CH_2NHCH_2CH_2N(CH_2CH_2NH_2)_2\}$ and one tertiary in the dimethylpropylamino tail $\{-CH_2CH_2CH_2N(CH_3)_2\}$. The extent of their protonation when **6b** is lodged in the minor groove is not obvious. In solution at pH 7.0, **6b** would be expected to have at least four of its five amino groups protonated.[2a,14] The upfield shift of the $CH_2^{R3}(3)$ resonance suggests protonation of the $-CH_2CH_2CH_2N(CH_3)_2$ nitrogen. The latter is involved in hydrogen bonding with $C_{11}O4'$. The deshielding of the tren polyamino end methylenes, $CH_2^{R2}(1')/(2')$, by <0.1 ppm is also suggestive of protonation of the corresponding terminal tren nitrogens involved in hydrogen bondings (the dominant effect on $\Delta\delta$) with the phosphate oxygens of T_9P and $G_{10}P$ as shown by the molecular modeling results (Figure 8). We have assumed (*vide infra*), in our restrained molecular modeling, that all five amino functions are fully protonated.[2a,14] This is in agreement with the induced chemical shift differences for the methylene protons flanking the involved amino groups (Table 1). When complexed to dsDNA, the four tren amino groups are intimately associated with two negatively charged phosphates, T_9P and $G_{10}P$.

Examination of the X-ray structure of the $d(CGCA_3T_3GCG)_2$:distamycin complex[15a] and the $d(CGCGAATT^{Br}CGCG)_2$:netropsin complex[16] leads to the conclusion that the minor groove can increase its width upon binding to lexitropsins. Using X-ray structures, comparison of the width (phosphate to phosphate at the A·T binding site) of the minor grooves of $d(CGCA_3T_3GCG)_2$[15b] (9.4–9.9 Å) and $d(CGCA_3T_3GCG)_2$:distamycin complex (9.4–10.8 Å)[15a] shows an increase of 0–0.9 Å. Using the NMR solution structures, comparison of the width of the minor grooves of $d(CGCA_3T_3GCG)_2$ (6.5–10 Å)[2e] and $d(CGCA_3T_3GCG)_2$:**6b** (9.2–9.6 Å) shows an increase of 0.4–3.1 Å.

There is some variability in the positioning of ligands within the minor groove of B-DNA even when there is a common motif such as the "flat sickle-shape" of **6b**, **5c**, and distamycin. Thus, the amide nitrogens of **6b** are embedded to a distance of 3.1–4.5 Å from the floor of the groove. The crystal structure of the $d(CGCA_3T_3GCG)_2$:distamycin complex[15] shows distamycin penetrating to within 4.2–4.5 Å from the bottom of the minor groove. Examination of Figure 8 shows how the positively charged dimethylpropylamino tail (R_3) of **6b** resides at a position which is adjacent to the $C_{11}O2$ and $C_{11}O4'$ in the minor groove, while the protonated tren moiety is paired with the phosphates of T_9 and G_{10}. The three primary amines of **6b**'s tren amino substituent are located within 1.75 Å of two phosphodiester oxyanions, while the fourth amine (tertiary) is 3.0 Å from the same two adjacent phosphodiester oxyanions. The binding of distamycin in the minor groove is enhanced by its amidine tail forming bifurcated hydrogen bonds to the bottom of the minor groove.[15] Changing the amidine tail $\{-CH_2CH_2C(=NH)NH_2\}$ of the carboxyl terminus of distamycin to a $-CH_2CH_2CH_2N(CH_3)_2$ group and the formyl substituent at the amino terminus to acetamide causes a decrease in the equilibrium constant for 1:1 complex formation with d(GGCGCA$_3$T$_3$GGCGG)/d(CCGCCA$_3$T$_3$GCGCC) from 4×10^7 for distamycin to 6×10^6 M^{-1}.[3] However, further change of the *N*-methyl group on its central pyrrole to include a four methylene linker and a tren polyamino side chain (**6b**) leads to a binding constant of 8×10^8 M^{-1} to the same oligomer.[3] This greater than 100-fold increase from 6×10^6 to 8×10^8 M^{-1} in the binding constant must be due to the electrostatic interactions of the polyamino side chain with the phosphodiester linkages.[3]

The significance of the central polyamino groups of **6b** can be seen when comparing the bending angle of the $d(CGCA_3T_3GCG)_2$:**6b** complex (22.2°) with the angles found in distamycin complexed (1:1 and 2:1) to $d(CGCA_3T_3GCG)_2$ (13.9 and 11.3°, respectively; Figure 9). The molecular contact surface area between $d(CGCA_3T_3GCG)_2$ and **6b** is 518 Å^2.

In the 1:1 complexes of the dodecamer $d(CGCA_3T_3GCG)_2$ with **6b**, **5c**,[2e] or distamycin,[5] exchange is between two equivalent (A_3T_3) binding sites *via* the "flip-flop" mechanism. The rate constant for exchange (which equals the off-rate) for **6b** (10 °C) is ca. 1.3 s^{-1}. This may be compared to 0.2 s^{-1} for distamycin at 30 °C.[5] Thus, the exchange rate with **6b** at identical A_3T_3 sites appreciably exceeds that for distamycin.

(14) Lowry, T. H.; Richardson, K. S. *Mechanism and Theory in Organic Chemistry*, 3rd ed.; Harper & Row: New York, 1987; p 311.

(15) (a) Coll, M.; Frederick, C. A.; Wang, A. H.-J.; Rich, A. *Proc. Natl. Acad. Sci. U.S.A.* **1987**, *84*, 8385. (b) Coordinates provided by C. A. Frederick prior to actual release.

(16) Kopka, M. L.; Yoon, C.; Goodsell, D.; Pjura, P.; Dickerson, R. E. *Proc. Natl. Acad. Sci. U.S.A.* **1985**, *82*, 1376.

Comparative Conclusions on 5c: and 6b:d(CGCA$_3$T$_3$GCG)$_2$ Solution Structures. Both microgonotropens **6b** and **5c** bind to the A + T-rich region of dsDNA[2e,6] involving one G·C residue flanking the A·T binding sites. Based solely on ^{1}H NMR structural determination, the following conclusions can be drawn. Unlike the case of **5c** bound to d(CGCA$_3$T$_3$GCG)$_2$ in which the –CH$_2$CH$_2$CH$_2$N(CH$_3$)$_2$ tail at the carboxyl terminus of **5c** extends out of the minor groove, this tail in **6b** is completely within the minor groove (Figure 8c). The positioning of ligands within the minor groove of B-DNA is different even when there is a common motif such as the "flat sickle-shape" of **6b** and **5c**. While the amide nitrogens of **5c** are embedded[2e] to a distance of 4.5–7.0 Å from the floor of the groove, the same nitrogens of **6b** bind 3.1–4.5 Å from the bottom of the minor groove. The nitrogens of the dien polyamine substituent of **5c** {–(CH$_2$)$_5$N[CH$_2$CH$_2$CH$_2$N(CH$_3$)$_2$]$_2$} pair with three phosphates of dsDNA, while those of the tren substituent of **6b** {–(CH$_2$)$_4$NHCH$_2$CH$_2$N(CH$_2$CH$_2$NH$_2$)$_2$} interact with two adjacent phosphates. The efficiency of binding of the tren substituent of **6b** (as seen by the embedding of the tripyrrole peptide in the minor groove) *vs* the dien substituent of **5c** can be ascribed to the smaller steric effect around the terminal amino groups of the tren allowing a better pairing with the phosphate backbone of dsDNA. This is consistent with the higher first equilibrium of binding of **6b** (8×10^8 M^{-1}) as compared to **5c** (2×10^8 M^{-1}) when bound to d(GGCGCA$_3$T$_3$GGCGG)/d(CCGCCA$_3$T$_3$GCGCC).[3] Tren-microgonotropen-b, **6b** (i) penetrates deeper into the minor groove of dsDNA than **5c**, (ii) exhibits a stronger interaction with the phosphate backbone as compared to **5c**, and (iii) has a hydrocarbon linker between the tripyrrole peptide and the tren substituent that is shorter than the linker in **5c**.

Comparison of the bending angles, α, of the solution structures of d(CGCA$_3$T$_3$GCG)$_2$ ($\alpha = 21.4°$), d(CGCA$_3$T$_3$GCG)$_2$:**6b** ($\alpha = 22.2°$), and d(CGCA$_3$T$_3$GCG)$_2$:**5c** ($\alpha = 17.2°$) reveals that **5c** decreases the bending angle[2e] of d(CGCA$_3$T$_3$GCG)$_2$ in solution by 4.2° and **6b** increases the angle by 0.8°. The molecular contact surface area between d(CGCA$_3$T$_3$GCG)$_2$ and **6b** is 10 Å^2 less than was found for the same DNA complexed with **5c**.[2e] Both **6b** and **5c** in the 1:1 complexes with the dodecamer d(CGCA$_3$T$_3$GCG)$_2$ exchange between two equivalent (A$_3$T$_3$) binding sites *via* the "flip-flop" mechanism with a rate constant of ca. 1.3 s^{-1}. Although some of the differences in the solution structures are quite small, the structural characteristics of the two dsDNA complexes provide the necessary tools for further ligand design.

Experimental Section

The synthesis of **6b** has been reported.[3] The self-complementary d(CGCAAATTTGCG)$_2$ was obtained by annealing[2d,6] the single stranded DNA oligomer prepared and purified at the Biomolecular Resource Center, University of California, San Francisco.

The NMR samples contained either 0.38 or 2.5 mM ($\mu = 0.079$ and 1.2, respectively) d(CGCA$_3$T$_3$GCG)$_2$ in 10 mM potassium phosphate buffer and 10 mM NaCl at pH 7.0 with 0.1% DSS in 0.4 mL of D$_2$O. Concentrations of ssDNA for d(CGCA$_3$T$_3$GCG) were determined from the absorbance at 260 nm ($\epsilon_{260,\text{single-stranded}} = 1.36 \times 10^5$ M^{-1} cm^{-1}, 60 °C). One equivalent of **6b** was added to 0.4 mL of 2.5 mM oligomer, and this sample was lyophilized twice from 99.9% D$_2$O, once from 99.96% D$_2$O, and finally dissolved in 0.4 mL of 99.96% D$_2$O (Aldrich) under a nitrogen atmosphere. (The titration sample was dried in an analogous manner in the absence of **6b**.) The solution was kept refrigerated at 4 °C between uses. All NMR spectra were recorded at 500 MHz on a GN-500 (General Electric) spectrometer at 10 °C, unless otherwise specified. Chemical shifts were referenced to the signal of DSS (2,2-dimethyl-2-silapentane-*3,3,4,4,5,5-d$_6$*-5-sulfonate; 0 ppm).

1D NMR. The titration experiment was performed in D$_2$O at 21 °C in 0.25 mol equiv steps of **6b**/d(CGCA$_3$T$_3$GCG)$_2$ at 3.8×10^{-4} M of d(CGCA$_3$T$_3$GCG)$_2$. Mesitoate (2,4,6-trimethylbenzoate) was present at 3.8×10^{-4} M as an internal standard. The melting study of dsDNA was performed at 3.8×10^{-4} M of d(CGCA$_3$T$_3$GCG)$_2$ between 20 and 60 °C with DSS as an internal standard. In the quantitations of the T$_7$CH$_3$ resonances during the melting study, the area of the impurity (triethylammonium acetate) was subtracted to calculate the normalized peak area ratios of T$_7$CH$_3$/DSS. The melting temperature of an oligomer can be estimated from $T_m = 4$(G·C)+2(A·T) where A·T and G·C represent the number of base pairs,[7a] or perhaps calculated more accurately from eq 1 where N is the chain length in bp and [Na$^+$] is the buffer and

$$T_m = 81.5 - 16.6(\log [Na^+]) + 0.41(\%G\cdot C) - 600/N, °C \quad (1)$$

added salt concentration in mM.[7b]

2D NMR. NOESY experiments were recorded in the phase sensitive mode using the hypercomplex NOE pulse sequence[17] with mixing times of 50, 100, and 180 ms for the d(CGCA$_3$T$_3$GCG)$_2$:**6b** complex. Spectra were collected into 4 K complex points for 512 t_1 increments with a spectral width of 5681 Hz in both dimensions. The data matrix was zero filled to 2 K and appodized with a Gaussian function to give a line broadening of 1 Hz in both frequency domains. The ROESY experiment was recorded at 10 °C using the Kessler pulse sequence[18] with a mixing time of 50 ms and a locking field strength of 2.5 kHz. The assignment of the ^{1}H chemical shifts generally followed the rules of assignment previously established.[10c,e]

Notations. Here, as elsewhere,[2e,10] the numbering of DNA protons follows the rule that the sugar protons will be denoted by prime and double prime superscripts and preceded by the name of the residue to which they belong. When reference is made to the same proton of more than one residue, all residues are listed followed by the proton type {e.g., A$_6$T$_7$T$_8$H2″ means the H2″ (sugar) protons which belong to the A$_6$, T$_7$, and T$_8$ residues; G$_2$G$_{10}$G$_{12}$H8 means the H8 (base) protons of the G$_2$, G$_{10}$, and G$_{12}$ residues}. When both H2′ and H2″ protons are involved in discussion, we used the H2′2″ abbreviation.

Distance calculations were made by measuring the volume integrals of the NOE enhancements from the 180 ms NOESY spectrum which were then related to interproton distances by eq 2 where r_a and

$$r_a = r_b(NOE_b/NOE_a)^{1/6}, Å \quad (2)$$

r_b are the distances corresponding to the unknown and known (C$_1$H5–C$_1$H6, 2.45 Å) interactions of a pair of protons with their corresponding NOE$_a$ and NOE$_b$.[19] The linearity of the NOE buildup with τ_m was checked for most of the dsDNA proton interactions between 50 and 180 ms, and a 5–20-fold increase was found in the NOE volume integrals from the 50 to 180 ms mixing times. The NOESY derived distances are generally defined by lower and upper bounds to reflect the uncertainties of the measurements. We set the differences between the upper and lower limits to 1 Å in the refinement of the structural data. The exchange rate (k_{ex}) was calculated from eq 3 using the ratio of peak

$$k_{ex} = \ln((1 + R)/2\tau_m(1 - R)), s^{-1} \quad (3)$$

intensities (R), expressed in number of contour levels (off diagonal/diagonal) from a short mixing time (τ_m) ROESY spectrum.[20] The free energy of activation, ΔG^*, for this exchange process at a certain temperature, T (K), was calculated from eq 4.[21]

$$\Delta G^* = 19.14T[10.32 - \log(k_{ex}/T)], J/mol \quad (4)$$

Computational analysis and restrained molecular modeling were performed on a Silicon Graphics (Mountain View, CA) Iris 4D/340GTX workstation using CHARMm[22] (version 21.3) and QUANTA (version 3.3.1) programs (Molecular Simulations, Waltham, MA). The solution structure of **5c** in a complex with d(CGCA$_3$T$_3$GCG)$_2$ was used as initial coordinates for **6b**.[2e] The aliphatic chain and dien polyamino group on the central pyrrole nitrogen of **5c** were replaced with a (CH$_2$)$_4$ methylene chain and a tren moiety {–NHCH$_2$CH$_2$N(CH$_2$CH$_2$NH$_2$)$_2$} using 3D Molecular Editor (QUANTA). Atomic partial charges of the atoms in

(17) States, D. J.; Haberkorn, R. A.; Ruben, D. J. *J. Magn. Reson.* **1982**, *48*, 286.
(18) Kessler, H.; Griesinger, C.; Kerssebaum, R.; Wagner, E.; Ernst, R. *J. Am. Chem. Soc.* **1987**, *109*, 607.
(19) Zhang, X.; Patel, D. J. *Biochemistry* **1990**, *29*, 9451.
(20) Ernst, R. R.; Bodenhausen, G.; Wokaun, A. *Principles of Nuclear Magnetic Resonances in One and Two Dimensions*; Clarendon Press: Oxford, 1987.
(21) Günther, H. *NMR Spectroscopy: An Introduction*; John Wiley: New York, 1980; p 241.
(22) Brooks, B. R.; Bruccoleri, R. E.; Olafson, B. D.; States, D. J.; Swaminathan, S.; Karplus, M. *J. Comput. Chem.* **1982**, *4*, 187.

6b and $d(CGCA_3T_3GCG)_2$ were generated from CHARMm's force field's parameter files. Primary, secondary, and tertiary amines were modeled as fully protonated with a total charge of +5 for **6b** (partial charge of +0.35 for each protonated amine of **6b**).

To the solution structure of the dodecamer,[2e] **6b** was docked into the minor groove to initiate structural refinement of the 1:1 complex of $d(CGCA_3T_3GCG)_2$:**6b**. CHARMm minimization was subsequently conducted exactly as previously described for **5c**[2e] {*in vacuo*; distance constraint forces ranged up to 500 kcal/mol·Å^2 depending upon the upper and lower limits for a given NOE derived value; a radially dependent distance dielectric with $\epsilon = R$ was used to account for solvent effects; the nonbonded cutoff distance was 15 Å, while the nonbonded and energy lists were updated every five steps; 100 steps of steepest descents minimization were followed by the adopted basis Newton-Raphson algorithm until the root mean square derivative reached <0.5 kcal/mol·Å} with the following exception: only 2 Na^+ gegenions (instead of 4 for the **5c** structure)[2e] were removed from vicinity of the phosphates nearest to where the protonated polyamine side chain and dimethylamine tail of **6b** were initially located. Molecular and helical parameters were also measured exactly as before.[2e,23] Dihedral angle constraints were not included in the simulations. The distances of **6b** to the DNA (-) and (+) strands were measured from the pyrrolic nitrogens to $P_{-4}P_{-5}P_{-6}$ and $P_8P_9P_{10}$, respectively. The depth of **6b** binding was defined by measuring the distances from the amide nitrogens N1, N2, and N3 to the lines connecting $T_{-6}O2$ and A_6H2, $A_{-7}H2$ and T_7O2, and $A_{-8}H2$ and T_8O2 atoms, respectively.

(23) NEWHEL93 was generously provided by R. E. Dickerson. The program was run on a VAXstation 3100 with coordinates in Brookhaven's Protein Data Bank format. The best helicies were generated from the sugars' C1′, the pyrimidine's N1, and the purine's N9 atoms. For more information on an earlier version of this program, see: Prive, G. G.; Yanagi, K.; Dickerson, R. E. *J. Mol. Biol.* **1991**, *217*, 177.

Acknowledgment. This work was supported by grants from the Office of Naval Research and the National Science Foundation.

Supplementary Material Available: Figure S1, DQF-COSY spectrum of **6b**, 5×10^{-3} M in D_2O at 21 °C; Figure S2, expansion of the DQF-COSY spectrum of the 1:1 complex in the (1.2–6.4) × (1.2–6.4) ppm region; Figure S3, expansion of the DQF-COSY spectrum of the 1:1 complex in the (3.6–4.9) × (3.6–4.9) ppm region; Figure S4, expansion of the DQF-COSY spectrum of the 1:1 complex in the (1.1–3.7) × (1.1–3.7) ppm region; Figure S5, expansion of the DQF-COSY spectrum of the 1:1 complex in the (4.5–6.3) × (1.6–2.9) ppm region; Figure S6, expansion of the NOESY spectrum of the 1:1 complex in the (3.3–6.9) × (3.3–6.9) ppm region; Figure S7, expansion of the NOESY spectrum of the 1:1 complex in the (1.0–3.4) × (1.1–3.4 ppm region; Figure S8, expansion of the NOESY spectrum of the 1:1 complex in the (3.6–5.2) × (6.9–8.5) ppm region; and Figure S9, ROESY spectrum of the 1:1 complex (11 pages). This material is contained in many libraries on microfiche, immediately follows this article in the microfilm version of the journal, and can be ordered from the ACS; see any current masthead page for ordering information.